



## Shedding light on surface exposition of poly(ethylene glycol) and folate targeting units on nanoparticles of poly( $\epsilon$ -caprolactone) diblock copolymers: Beyond a paradigm



Alessandro Venuta<sup>a,1</sup>, Francesca Moret<sup>b,1</sup>, Giovanni Dal Poggetto<sup>c,1</sup>, Diletta Esposito<sup>a</sup>, Aurore Fraix<sup>d</sup>, Concetta Avitabile<sup>e</sup>, Francesca Ungaro<sup>a</sup>, Mario Malinconico<sup>c</sup>, Salvatore Sortino<sup>d</sup>, Alessandra Romanelli<sup>a,e</sup>, Paola Laurienzo<sup>c</sup>, Elena Reddi<sup>b</sup>, Fabiana Quaglia<sup>a,\*</sup>

<sup>a</sup> Drug Delivery Laboratory, Department of Pharmacy, University of Napoli Federico II, Via Domenico Montesano 49, 80131 Napoli, Italy

<sup>b</sup> Department of Biology, University of Padova, Via Ugo Bassi 58/B, 35121 Padova, Italy

<sup>c</sup> Institute for Polymers, Composites and Biomaterials, CNR, Via Campi Flegrei 34, 80078 Pozzuoli, Napoli, Italy

<sup>d</sup> Laboratory of Photochemistry, Department of Drug Science, Viale Andrea Doria 6, 95125 Catania, Italy

<sup>e</sup> Institute of Biostructure and Bioimaging, CNR, via Mezzocannone 16, 80134 Napoli, Italy

### ARTICLE INFO

#### Keywords:

Biodegradable nanoparticles, poly(ethylene glycol)  
Folate  
Protein interaction  
Cell uptake

### ABSTRACT

Polymeric nanoparticles (NPs) of poly( $\epsilon$ -caprolactone) (PCL) covered with a hydrophilic poly(ethylene glycol) (PEG) shell are usually prepared from diblock PEG-PCL copolymers through different techniques. Furthermore PEG, NPs can be decorated with targeting ligands to accumulate in specific cell lines. However, the density and conformation of PEG on the surface and its impact on the exposition of small targeting ligands has been poorly considered so far although this has a huge impact on biological behaviour. Here, we focus on PEG-PCL NPs and their folate-targeted version to encourage accumulation in cancer cells overexpressing folate receptor  $\alpha$ . NPs were prepared with mixtures of PEG-PCL with different PEG length (short 1.0 kDa, long 2.0 kDa,) and a folate-functionalized PEG-PCL (PEG 1.5 kDa) by the widely employed solvent displacement method. In depth characterization of NPs surface by <sup>1</sup>H NMR, fluorescence and photon correlation spectroscopy evidenced a PEGylation extent below 7% with PEG in a mushroom conformation and the presence of folate more exposed to water pool in the case of copolymer with short PEG. NPs with short PEG adsorbed HSA forming a soft corona without aggregating. Although limited, PEGylation overall reduced NPs uptake in human macrophages. Uptake of NPs exposing folate prepared with short PEG was higher in KB cells (FR +) than in A549 (FR -), occurred via FR-receptor and involved lipid rafts-dependent endocytosis. In conclusion, the present results demonstrate that PEG length critically affects protein interaction and folate exposition with a logical impact on receptor-mediated cell uptake. Our study highlights that the too simplistic view suggesting that PEG-PCL gives PEG-coated NPs needs to be re-examined in the light of actual surface properties, which should always be considered case-by-case.

### 1. Introduction

Polymeric nanoparticles (NPs) are in the limelight in cancer nanotechnology due to the advantages of prompt manipulation of the overall features (size, surface hydrophilicity/charge, release rate, biodegradability) through appropriate tailoring of the chemistry of building blocks (Grossen et al., 2017). Amid the huge amount of biomaterials developed so far, poly( $\epsilon$ -caprolactone)-poly(ethylene glycol) PEG-PCL copolymers with different hydrophilic/lipophilic balance and

architectures have been synthesized resulting in a wide arsenal for drug delivery application (Li and Tan, 2014). In the context of cancer therapies, NPs of PEG-PCL block copolymers have gained attention in preclinical studies and in clinical settings with the promise to ameliorate chemotherapy outcome and decrease treatment toxicity. As far as PEG-PCL NPs for intravenous injection are concerned, a PEGylated surface can help to escape Mononuclear Phagocyte System (MPS), to attain long-circulation and to promote extravasation in inflamed tissues with a typical dysfunctional capillary bed such as in tumors (Bertrand

\* Corresponding author.

E-mail address: [quaglia@umina.it](mailto:quaglia@umina.it) (F. Quaglia).

<sup>1</sup> These authors equally contributed.

and Leroux, 2012). While demonstrating excellent stability in PBS, PEG-PCL NPs were even found to aggregate in the presence of serum (Gao et al., 2014).

Surface modification of PEGylated NPs with covalently-linked small ligands is a further strategy followed to increase drug level in cancer cells. To this purpose, the design of folate-decorated NPs carrying a chemotherapeutic and internalizing in cancer cells through FR $\alpha$ -mediated endocytosis has become a hot topic (Cheung et al., 2016). FR $\alpha$  expression level is a marker of tumor aggressiveness, plays a role in the low response rate to chemotherapeutics resistance and is insensitive to chemotherapy regimen (Cheung et al., 2016), thus strengthening the potential utility of FR-mediated delivery. Folate decoration of PEG-PCL NPs has been attempted by us and other authors by synthesizing all-in-one amphiphilic block copolymers bearing folate at PEG hydroxyl-end group and able to form core-shell NPs (Grossen et al., 2017). When the amphiphilic diblock polymers self-assemble into NPs in an aqueous phase, the PEG segments are expected to form the outer corona allowing the conjugated folic acid to become fully accessible on the surface. In contrast to this paradigm, we observed that for highly PEGylated micelle-like NPs, folate exposition in the presence of serum is highly dependent by the formation of a protein corona (Conte et al., 2016).

Another aspect to consider when fabricating PEG-PCL NPs refers to the mode of copolymer assembly. While dialysis has been largely employed to prepare PEG-PCL micelles/NPs, scale-up of production as well as in-process sterilization is feasible with microfluidics which takes after solvent displacement (nanoprecipitation) techniques. Importantly, mode of assembly of PEG-PCL copolymers can highly affect the amount of PEG on the surface (Quaglia et al., 2006) while its impact on protein adsorption and targeting features has been poorly considered.

On this basis, it is evident that PEG coverage plays a crucial role in controlling the biological fate of PEGylated NPs with an huge impact on the processes driven by protein interactions (immune system recognition, biodistribution), transport through biological matrices (tumor extracellular matrix, mucus, bacteria biofilm), and target recognition and docking (cell uptake) (Rabanel et al., 2014). Despite the extensive use of PEG, there is no consensus on the target product profile in term of PEG density, molecular weight and conformation when developing PEGylated NPs intended for a specific application, in cancer as well (Owens and Peppas, 2006). Thus, surface of NPs should be characterized in depth through complimentary techniques in view of a full optimization of the nanocarrier and following clinical application (Rabanel et al., 2014).

In this study, we try to shed light on the surface exposition of PEG and folate targeting units on NPs of PEG-PCL diblock copolymers prepared by solvent displacement technique and to relate shell features to uptake in human cells. To this purpose, we synthesized PEG-PCL copolymers with either 1 kDa or 2 kDa PEG chains and a Fol-PEG-PCL copolymers with 1.5 kDa PEG segment. Shell properties of untargeted and folate-targeted NPs were fully characterized through complementary techniques, such as  $^1\text{H}$  NMR, fluorescence, photon correlation spectroscopy and  $\xi$  potential. The impact of shell features on NPs interaction with human serum albumin, stability in biologically-relevant media as well as internalization in human macrophages and cancer cells overexpressing folate receptor were investigated.

## 2. Experimental section

### 2.1. Materials

Poly(ethylene glycol) (PEG) with Mn 1.5 kDa (PEG1.5k, Sigma-Aldrich, Milan, Italy), monomethoxy-poly(ethylene glycol) with Mn 2.0 kDa (mPEG<sub>L</sub>, Sigma-Aldrich, Italy) and monomethoxy-poly(ethylene glycol) with Mn 1.0 kDa (mPEG<sub>S</sub>, Nanocs Inc., USA) were dehydrated by azeotropic distillation with dry toluene in a Dean-Stark trap.  $\epsilon$ -Caprolactone (CL, Sigma-Aldrich, Italy) was distilled over CaH<sub>2</sub> under

vacuum. Stannous-(2-ethylhexanoate)<sub>2</sub> (Sn(oct)<sub>2</sub>), *N*-hydroxysuccinimide (NHS), *N,N'*-dicyclohexylcarbodiimide (DCC), triethylamine (TEA), dimethylaminopyridine (DMAP), tosyl chloride (TsCl), folic acid (Fol), propargylamine, triphenylphosphine (PPh<sub>3</sub>), silver(I) oxide, potassium iodide and sodium azide were used without further purification. Copper wires (Carlo Erba, Italy) were treated with H<sub>2</sub>SO<sub>4</sub> for 3 min, washed with water and methanol, and finally dried under vacuum in an oven for 30 min at 60 °C. 1,4-Butandiol, 1-hexanol, *N,N*-dimethylformamide (DMF) and dichloromethane (DCM) were dried before use according to standard procedures. All the other solvents (analytical grade) were purchased from Sigma-Aldrich and used as received. (2-Hydroxypropyl)- $\beta$ -cyclodextrin (HP $\beta$ CD, DS 0.9), Nile Red (NR) and Human Serum Albumin (HSA) were from Sigma (Italy).

### 2.2. Copolymer characterization

FTIR analysis was performed with a Perkin-Elmer spectrometer (Paragon 500) equipped with a ZnSe attenuated total reflectance (ATR) crystal accessory. Samples were placed in direct contact with the ATR crystal and pressed with a pressure clamp positioned over the crystal/sample area to allow intimate contact between the material and the crystal. Spectra were acquired in the 4000–400 cm<sup>-1</sup> range, at a resolution of 2 cm<sup>-1</sup> (average of 20 scans).  $^1\text{H}$  NMR analysis, spectra were recorded with a Bruker Avance DPX400 apparatus operating at 400 MHz. For GPC analysis, samples were dissolved in THF and passed through a 0.22  $\mu\text{m}$  PTFE membrane filter. Measurements were performed on an injected volume of 100  $\mu\text{L}$  by using a Malvern-Viscotek GPC MAX/TDA 305 quadruple detector array equipped with a pre-column and two Phenogel columns (Phenomenex) with exclusion limits 10<sup>6</sup> and 10<sup>3</sup> respectively. The GPC instrument was used at a flow rate of 0.8 mL/min and at columns and system temperature of 35 °C. Triple detectors calibration was based on a standard of polystyrene with molecular weight 104,959 Da. Residual copper content was estimated by Microwave Plasma-Atomic Emission Spectrometry (MP-AES) with a Agilent 4100 spectrometer. A microwave digestion system Milestone Ethos Touch Control was used for digestion of sample. The finely ground sample (0.1 g) was transferred in a teflon microwave digestion vessel and treated with 6 mL of HNO<sub>3</sub>, 3 mL of HCl and 1 mL of H<sub>2</sub>O<sub>2</sub> (Ultrapure Reagents, trace metal grade < 1  $\mu\text{g/L}$ ). The samples were processed by microwave digestion as follows: ramp to 200 °C over 10 min, then hold at 200 °C for 20 min. After digestion, the samples were cooled to room temperature, filtered, transferred in a 50 mL volumetric flask and adjusted to 50 mL with distilled water for spectrometric analysis. The amount of Fol linked to the copolymer was quantified by UV-vis spectroscopy on DMSO polymer solutions (0.2–2 mg/mL), using Fol standard solutions in DMSO to construct calibration curves. The absorbance of the sample was evaluated at 360 nm on a Shimadzu 1800 spectrophotometer.

### 2.3. Synthesis of mPEG<sub>S</sub>-PCL and mPEG<sub>L</sub>-PCL

Linear diblock copolymers were prepared by ring-opening polymerization (ROP) of CL at 120 °C for 24 h using mPEG<sub>L</sub> or mPEG<sub>S</sub> as initiator and Sn(Oct)<sub>2</sub> as catalyst (20%). CL/initiator molar ratio = 36.  $^1\text{H}$  NMR (CDCl<sub>3</sub>,  $\delta$  in ppm), PCL block: 1.29–1.78 (m), 2.19–2.43 (t) 3.20 (m); 3.92–4.21 (t), 4.31(t); PEG block: 4.10 (t), 3.64 (s), 3.38, (t).

### 2.4. Synthesis of Fol-PEG-PCL

#### 2.4.1. Synthesis of azido-PEG-PCL copolymer (N<sub>3</sub>-PEG-PCL)

Step 1. Synthesis of monotosyl-PEG (Ts-PEG-OH). PEG (5.00 g, 3.34 mmol) was dissolved in 50 mL of dry toluene. Ag<sub>2</sub>O (1.161 g, 5.01 mmol) and KI (110 mg, 0.668 mmol) were finely dispersed in the solution by stirring, then TsCl (2.76 g, 14.5 mmol) was added. The reaction mixture was kept at room temperature under stirring and nitrogen atmosphere for 12 h. The solution was filtered and solvent

removed by rotary evaporation. The polymer was dissolved in 10 mL of DCM and precipitated in cold diethyl ether (yield 95%).  $^1\text{H}$  NMR (d<sub>6</sub>-DMSO,  $\delta$  in ppm): 7.79 (2H, d), 7.49 (2H, d), 4.56 (1H, t), 4.11 (2H, t), 3.49 (128H, s), 2.43 (3H, s). Step 2. Synthesis of monoazido-PEG (N<sub>3</sub>-PEG-OH). Ts-PEG-OH (1.00 g, 0.66 mmol) was dissolved in 15 mL of dry DMF, then NaN<sub>3</sub> (214 mg, 3.3 mmol) was added and the mixture was stirred at 90 °C overnight under nitrogen atmosphere. The reaction mixture was cooled to room temperature, filtered, and DMF removed under vacuum. The product was dissolved in 10 mL of DCM and the solution was extracted twice with brine and twice with water in a separating funnel. The organic phase was dried over anhydrous Na<sub>2</sub>SO<sub>4</sub>, concentrated and poured in cold diethyl ether. Polymer was collected by filtration (yield 81%).  $^1\text{H}$  NMR (d<sub>6</sub>-DMSO,  $\delta$  in ppm): 4.56 (1H, t), 3.6 (2H, t), 3.5 (127H, s, PEG backbone), 3.4 (2H, t). FTIR diagnostic band: 2107 cm<sup>-1</sup> (N<sub>3</sub> stretching). Step 3. Synthesis of N<sub>3</sub>-PEG-PCL copolymer. N<sub>3</sub>-PEG-OH (600 mg, 0.393 mmol), CL (1.572 g, 13.77 mmol) and Sn(Oct)<sub>2</sub> (31 mg, 0.078 mmol) were charged in a flask under dry nitrogen. The polymerization was carried out at 120 °C for 24 h under stirring. The copolymer was dissolved in 10 mL of DCM, precipitated in cold hexane, recovered by filtration and finally dried (yield 91%).  $^1\text{H}$  NMR (CDCl<sub>3</sub>,  $\delta$  in ppm): 3.6 (2H, t), 3.5 (127H, s, PEG backbone), 3.4 (2H, t), 1.29–1.78 (139H, m); 2.19–2.43 (82H, m), 3.92–4.21 (82H, t), 4.31 (2H, t); Mn of PCL evaluated by  $^1\text{H}$  NMR = 4,6 kDa.

#### 2.4.2. Synthesis of propargylfolate

Fol (500 mg, 1.13 mmol) was charged in a flask under dry nitrogen and dissolved by stirring in 20 mL of DMSO over mild heating, then DCC (446 mg, 2.16 mmol) and NHS (260 mg, 2.26 mmol) were added. Reaction was carried out in the dark at room temperature for 17 h, the solution was filtered to remove the side product (dicyclohexylurea, DCU), then propargylamine (124 mg, 2.25 mmol) and TEA (228 mg, 2.25 mmol) were added. The reaction was left overnight. The product was precipitated with a diethylether/acetone 80/20 mixture, repeatedly washed first with acetone and then with diethylether, and finally dried under vacuum overnight. A yellow powder was obtained and analyzed by LC-MS (Agilent Technologies, 6230 ESI-TOF) on a Phenomenex Jupiter column (C18, 3  $\mu\text{m}$ , 150  $\times$  2.0 mm) with a gradient of acetonitrile (0.1% TFA) in water (0.1% TFA), from 5 to 50% in 15 min at a flow rate of 0.2 mL/min.

#### 2.4.3. Click conjugation of propargylfolate with N<sub>3</sub>-PEG-PCL (Fol-PEG-PCL)

N<sub>3</sub>-PEG-PCL (800 mg, 0.12 mmol) dissolved in 15 mL of DMSO was charged in a flask under dry nitrogen, then propargylfolate (86 mg, corresponding to a propargyl/N<sub>3</sub> molar ratio of 1.1) and copper wires (120 mg) were added; the reaction was carried out under stirring at room temperature overnight. The solution was filtered to remove copper and then dialyzed against DMSO with a 2000 cut-off dialysis tube for 4 days, in order to eliminate free propargylfolate and other side products. Finally, DMSO was evaporated under nitrogen stream. The occurrence of reaction was confirmed by FTIR through the complete disappearance of 2097 cm<sup>-1</sup> N<sub>3</sub> stretching band (yield 95%). Fol content = 6.5% by wt, functionalization degree = 90%.

#### 2.5. Preparation and characterization of nanoparticles

Non-targeted NPs were prepared from mPEG<sub>5</sub>-PCL and mPEG<sub>1</sub>-PCL while folate-decorated NPs were prepared from a mixture of mPEG<sub>5</sub>-PCL or mPEG<sub>1</sub>-PCL with Fol-PEG-PCL. NPs were formed by solvent diffusion of an organic phase (10 mg of copolymer in 1 mL of acetone) added dropwise in water (2 mL) under magnetic stirring (500 rpm). After solvent evaporation, NPs were filtered through 0,45  $\mu\text{m}$  Phenex® filters (Phenomenex, USA). NPs could be freeze-dried (Modulyo Edwards) after the addition of HP $\beta$ CD as cryoprotectant (polymer: HP $\beta$ CD 1:10 wt. ratio, sample frozen in liquid N<sub>2</sub>, condenser

temperature – 55 °C) and stored at 4 °C. Recovery yield of the production process was evaluated on an aliquot of NPs without cryoprotectant by weighing the solid residue after freeze-drying. To evaluate cell uptake, the lipophilic dye NR was physically entrapped (0.2% of copolymer weight). The hydrodynamic diameter (D<sub>H</sub>), polydispersity index (PI) and zeta potential ( $\xi$ ) of NPs were determined on a Zetasizer Nano Z (Malvern Instruments Ltd).

Fixed aqueous layer thickness (FALT) of NPs was measured by monitoring the influence of ionic strength on  $\xi$ . Different amounts of NaCl stock solutions were added to NPs dispersed in water (5 mg/mL, 100  $\mu\text{L}$ ) and zeta potential of the samples measured. A plot of  $\ln \xi$  against  $3.33[\text{NaCl}]^{0.5}$  gives a straight line where the slope represents the thickness of the shell in nm. (Endres et al., 2011)  $^1\text{H}$  NMR was carried out on NPs dispersions to evaluate the amount of PEG on the surface. Spectra were recorded for either NPs prepared in D<sub>2</sub>O or NPs freeze-dried without cryoprotectant dissolved in d<sub>6</sub>-DMSO (5 mg/mL). Steady state fluorescence spectra were carried out with a RF6000 spectrofluorimeter (Shimadzu, Japan). Fluorescence lifetimes were recorded with Fluorolog-2 spectrofluorimeter (Model F111, Horiba) equipped with a TCSPC Triple Illuminator. The samples were irradiated by pulsed diode excitation source Nanoled at 370 nm. The kinetics were monitored at 450 nm and each solution was used to register the prompt at the excitation wavelength. The system allowed measurement of fluorescence lifetimes from 200 ps. The multiexponential fit of the fluorescence decay was obtained using the following equations:

$$I(t) = \alpha_1 \exp(-t/\tau_1) + \alpha_2 \exp(-t/\tau_2).$$

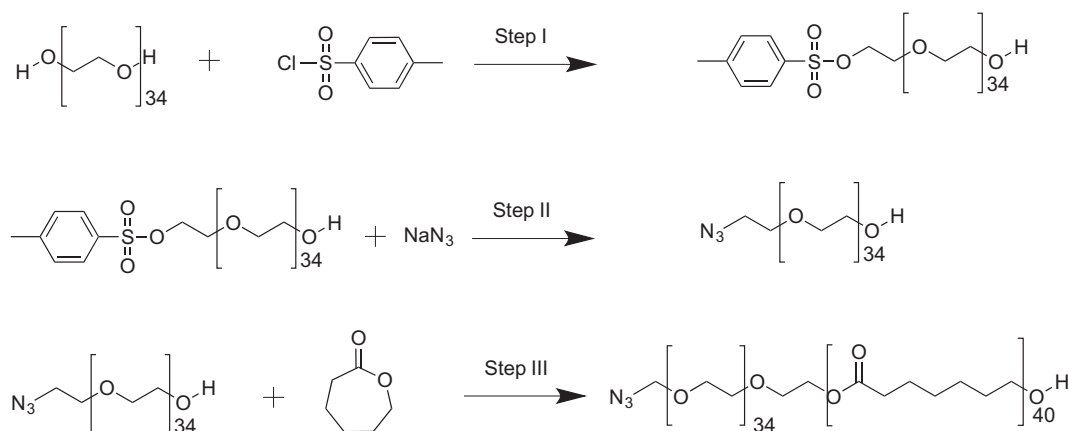
All measurements were performed in a thermostated quartz cell (1 cm path length, 3 mL capacity).

Stability of NPs in the presence of HSA (1–500  $\mu\text{M}$ ) was evaluated by placing a NPs sample (0.05 mg/mL) in the HSA water solution and monitoring immediately the size distribution by PCS.

#### 2.6. Intracellular uptake of NPs in cancer cells

KB carcinoma cells (American Type Culture Collection, ATCC, Rockville, USA) over-expressing FR (FR $\alpha$ ) were selected to study the specific internalization of Fol-decorated NPs vs. non-targeted NPs. The cells were grown in Eagle's medium (MEM) (Life Technologies) supplemented with 10% fetal bovine serum (FBS) (Gibco), 100 U/mL Penicillin G and 100  $\mu\text{g}/\text{mL}$  Streptomycin and maintained at 37 °C in a humidified atmosphere containing 5% CO<sub>2</sub>. Flow cytometry measurements of the uptake of DBL<sub>S</sub>, DBL<sub>S</sub>/DBL-Fol, DBL<sub>L</sub>, DBL<sub>L</sub>/DBL-Fol were performed using fluorescent NR-loaded NPs. For all the experiments mentioned above, cells were seeded in 24 wells/plate (40,000 cells/well) in folate-deficient RPMI medium (Life Technologies) supplemented with 10% FBS. After 24 h of growth at 37 °C, the cells were incubated for 1 h with 20  $\mu\text{g}/\text{mL}$  of NR-loaded NPs, freshly re-suspended in milliQ water and diluted in RPMI medium with or without 10% of FBS. After incubation with NPs, the cells were washed, detached from the plates with trypsin (Life Technologies), centrifuged and re-suspended in Versene before measuring NR fluorescence using a BD FACSCanto™ II instrument (Becton Dickinson). The blue laser at 488 nm was used as excitation source and the PerCP channel (670–735 nm) was selected for the detection of NR fluorescence. 10<sup>4</sup> events/sample were acquired and analyzed with the FACSDiva Software. Competition experiments with 1 mM free Fol were carried out incubating the cells for 1 h prior to the addition of NPs in order to saturate FRs exposed on cell surface. The intracellular uptake of NR loaded DBL<sub>S</sub> and DBL<sub>S</sub>/DBL-Fol was measured also in A549 cells (ATCC), negative for FR expression. The cells were grown in F12-K medium (Life Technologies) supplemented with 10% FBS, 100 U/mL Penicillin G and 100  $\mu\text{g}/\text{mL}$  Streptomycin. For the uptake experiments, cells were seeded as described above for KB cells and incubated for 1 h with NP formulations in the absence of serum in the incubation medium.

To assess the endocytosis mechanism of DBL<sub>S</sub>/DBL-Fol NPs, KB cells



**Scheme 1.** Synthetic pathway for synthesis of N<sub>3</sub>-PEG-PCL diblock copolymer. Monofunctionalization of PEG was checked by <sup>1</sup>H NMR analysis through the ratios between the intensities of –OH (4.56 δ) and –CH<sub>2</sub>–O–Ts (4.11 δ) protons of PEG, and aromatic (7.79, 7.49 δ) and –CH<sub>3</sub> (2.43 δ) protons of tosyl group (step 1).

were incubated 30 min before and during NP incubation (1 h) with specific molecules (all from Sigma) able to inhibit clathrin-mediated endocytosis (chlorpromazine hydrochloride, 5 μg/mL), caveolae-independent lipid-raft-dependent endocytosis (methyl-β-cyclodextrin, MβCD, 1 mM), caveolae-dependent endocytosis (Genistein 54 μg/mL and Filipin III 5 μg/mL).

The internalization of NPs in KB cells pre-incubated or not with 1 mM free Fol was assessed also by confocal microscopy using a SP5 laser scanning microscope (Leica Microsystems). 6 × 10<sup>4</sup> cells were seeded in special tissue culture dishes for fluorescence microscopy (μ-Dish 35 mm, high, Ibidi GmbH), were allowed to grow for 24 h and then incubated for 1 h with 20 μg/mL NPs in medium added with 10% FBS. After incubation, the cells were washed twice with PBS with Ca<sup>2+</sup> and Mg<sup>2+</sup> and immediately visualized under the microscope.

### 2.7. Capture of NPs by human macrophages

The capture by human macrophage of NPs decorated or not with Fol and pre-incubated in human serum (HS) was measured in order to assess their stealth properties. A positive control of non-PEGylated NPs (PCL) was tested too. Macrophages were derived from monocytes isolated from buffy coats of healthy donors by centrifugation over a Ficoll-Hypaque step gradient and subsequent Percoll gradient (Sigma-Aldrich). 2 × 10<sup>6</sup> isolated monocytes/well were seeded in 24 wells/plate and cultured for 7 days in RPMI 1640 medium (Life Technologies) supplemented with 20% FBS and 100 ng/mL of human macrophage colony-stimulating factor (Peprotech) to promote macrophage differentiation. On day 4 from the seed, the macrophage colony-stimulating factor was added again. For the uptake experiment, macrophages were incubated for 3 h in RPMI added with 10% FBS and 20 μg/mL fluorescent NPs previously incubated at 37 °C in human serum type AB (Sigma-Aldrich) for 0, 10 or 30 min. Macrophages were then washed and detached from the plates using PBS with 5 mM EDTA, centrifuged, re-suspended in PBS + 1% BSA and analyzed by flow cytometry for fluorescence as described previously. Propidium Iodide (1 μg/mL) staining of the samples during flow cytometry acquisition was used to measure the macrophage viability, which was higher than 95%.

### 2.8. Statistical analysis

The Primer software for biostatistics (McGraw-Hill, Columbus, USA) was used for statistical analysis of the data. The data are expressed as means ± SD of at least 3 independent experiments. The difference between groups was evaluated using the Student's *t*-test considered significant for *p* < 0.05.

## 3. Results and discussion

### 3.1. Synthetic strategy

The following PEG-PCL diblock copolymers with different PEG lengths were synthesized: i) Fol-PEG-PCL copolymer (PEG MW = 1.5 kDa); ii) mPEG-PCL with a PEG MW = 1.0 kDa (mPEG<sub>S</sub>-PCL); iii) mPEG-PCL with a PEG MW = 2.0 kDa (mPEG<sub>L</sub>-PCL). Copolymers were synthesized by typical ROP polymerization of ε-caprolactone using a mono-hydroxyl PEG as initiator. The molecular weight of PCL block was controlled by the CL/initiator molar ratio in the feed. A value of around 4.0 kDa was fixed for PCL on the basis of previous works (Conte et al., 2016; Tirino et al., 2014; Ungaro et al., 2012).

To prepare Fol-PEG-PCL copolymer, Cu(I)-catalyzed 1,3-Huisgen cycloaddition (“click” reaction) was chosen to conjugate folate to PEG-PCL (Himo et al., 2005). 1,3-Huisgen cycloaddition is the addition of alkynes to azides, with formation of highly stable 1,2,3-triazoles. The reaction is high yielding, stereospecific, does not create any byproduct, and can be conducted in mild conditions. PEG was first modified by introduction of an azide on one terminal group (Scheme 1). Synthetic strategies aimed to asymmetrically modify PEG are largely explored in the literature. In general, the reported methods suffers from a complex chemistry and/or low purity of the final product (Li and Chau, 2010; Szekely et al., 2014). The most common way to synthesize heterotelechelic PEG remains polymerization of ethylene oxide from different initiators (Cammis et al., 1995; Hiki and Kataoka, 2007; Ishii et al., 2005; Raynaud et al., 2009; Thompson et al., 2008). To achieve monofunctionalization, the use of a large excess of PEG has been reported too (El-Gogary et al., 2014) although separation of non-modified from modified polymer requires tedious chromatography and yields are generally low. In the present paper, we used a method recently reported (Mahou and Wandrey, 2012) to achieve asymmetric activation of low molecular weight alcohols to low molecular weight PEG, so that it becomes possible to selectively link a biomolecule of interest to one end of PEG, and use the residual –OH for copolymerization.

N<sub>3</sub>-PEG-OH is used as initiator for ring-opening polymerization of CL, leading to a PEG-azido functionalized copolymer. Azide is stable at the temperature required by ROP (120 °C), as confirmed through FTIR analysis, where no change of diagnostic band of azide at 2097 cm<sup>-1</sup> is detected in the copolymer spectrum. Mn of PCL block in the copolymers was calculated by the ratio between intensities of the resonance associated to –CH<sub>2</sub>–OH methylene protons at 3.64 δ and –CH<sub>2</sub>–CO– units in the PCL chain at 2.31 δ of <sup>1</sup>H NMR spectrum. A good agreement between theoretical and experimental values is found (Table 1).

In order to introduce the complementary alkyne group for successive coupling to N<sub>3</sub>-PEG-PCL, folic acid was conjugated with

**Table 1**  
Theoretical and experimental molecular weights of copolymers.

Sample	Mn (Da) <sup>a</sup>	Mn (Da) <sup>b</sup>	Mn (Da) <sup>c</sup>	Mw (Da) <sup>c</sup>	PDI <sup>d</sup> (Mw/Mn)
N <sub>3</sub> -PEG-PCL	5547	6203	5943	8049	1.36
mPEG <sub>S</sub> -PCL	5047	5446	5059	6737	1.33
mPEG <sub>L</sub> -PCL	6047	6579	6594	8720	1.35

<sup>a</sup> Theoretical number-average molecular weight.

<sup>b</sup> Number-average molecular weight evaluated by <sup>1</sup>H NMR.

<sup>c</sup> Molecular weight obtained by GPC.

<sup>d</sup> Molecular weight polydispersity index obtained by GPC.

propargylamine through carbodiimide chemistry. It is known from the literature that only  $\gamma$ -folate conjugates retain affinity towards the receptor (Chen et al., 2013). Remarkably,  $\gamma$ -conjugates are intrinsically obtained as the major product in reactions with carbodiimide (Viola-Villegas et al., 2008); nevertheless, a clean product is hard to obtain, as separation of  $\gamma$ -conjugate from  $\alpha$ - and bis-conjugates and unreacted folic acid is troublesome. For this reason, it is critical to find reaction conditions under which formation of “clickable”  $\alpha$ - and bis-conjugates is minimized. In this case, the crude product can be used as such for coupling with N<sub>3</sub>-PEG-PCL, then the final Fol-PEG-PCL copolymer will be easily separated from non-conjugated folic acid and other by-products (i.e., activated folic acid, Fol-NHS) by dialysis (Liu et al., 2012). For purposes of optimization, a screening at different reaction conditions (type and amount of catalyst and propargylamine/catalyst molar ratio) was preliminary carried out, and products were characterized by LC-MS (Table S1, Fig. S1). Identification of  $\alpha$ - and  $\gamma$ -conjugate peaks was made according to literature (Trindade et al., 2014). Conditions for  $\gamma$ -propargylfolate synthesis were set so that only a negligible amount of  $\alpha$ -conjugate and no bis-conjugate are formed (see Entry 1 of Table S1).

In the click reaction, copper in form of wires was preferred as catalyst, since concentration of Cu(I) ions in solution is very low with respect to other catalysts type (Nahrwold et al., 2013), avoiding long purification steps. The total amount of crude propargylfolate was calculated in order to have a propargyl/N<sub>3</sub> molar ratio corresponding to 1.1. Finally, the copolymer was easily purified by extensive dialysis to remove non-conjugated molecules. Reaction was followed by FTIR; the absence of azide band in the spectrum of Fol-PEG-PCL accounts for a 100% conversion (Fig. S2). For sake of accuracy, Fol-PEG-PCL was analyzed by GPC-UV. The chromatogram shows a single peak at a retention time corresponding to that of pristine N<sub>3</sub>-PEG-PCL copolymer, confirming the absence of free folic acid and/or derivatives (Fig. S3). As a final check, the amount of residual copper in the copolymer, determined by MP-AES analysis, was as low as 12 ppm, allowing to exclude any possible cytotoxic effect (Cao et al., 2012).

### 3.2. Influence of PEG length on nanoparticle shell

We aimed at studying the effect of PEG length on the shell properties of folate-decorated NPs. To this purpose, NPs based on mixtures of Fol-PEG-PCL with either mPEG<sub>S</sub>-PCL (DBL<sub>S</sub>/DBL-Fol), where PEG is 1.0 kDa, or mPEG<sub>L</sub>-PCL (DBL<sub>L</sub>/DBL-Fol), where PEG is 2.0 kDa, were prepared (Fig. 1). We fixed Fol-PEG-PCL amount in the composition at 20% by wt based on the results obtained in a previous paper (Conte et al., 2016). Corresponding non-targeted NPs were prepared from mPEG<sub>L</sub>-PCL (DBL<sub>L</sub>) and mPEG<sub>S</sub>-PCL (DBL<sub>S</sub>). Solvent diffusion method, currently indicated as nanoprecipitation, was selected since it is very popular for preparing biodegradable NPs. Furthermore, solvent diffusion is a working principle in microfluidics, a process useful to increase the scale of NP production.

As can be seen in Table 2, monodispersed NPs spontaneously form in good yield (around 60%) without the help of any surfactant. DBL<sub>L</sub> are smaller than DBL<sub>S</sub> likely due to higher hydrophilicity of mPEG<sub>L</sub>-PCL. A size lower than 100 nm as determined by dynamic light scattering and

comprised in a narrow size range (PI < 0.22) makes this formulation suitable for intravenous injection.  $\xi$  is slightly negative as commonly found for PEGylated NPs and slightly decreased for DBL<sub>S</sub>/DBL-Fol. NPs exhibit spherical morphology and preserve their shape once freeze-dried in the presence of HP $\beta$ CD (Fig. S4, Supplementary material).

The amount of PEG on NPs surface was evaluated by <sup>1</sup>H NMR and the packing extent of PEG on the surface calculated (Auguste et al., 2006; Xu et al., 2015). Results are reported in Table 2. For all the samples, the experimental amount of PEG on the surface is much lower than the theoretical value, suggesting that, in the conditions adopted to produce non-targeted and folate-targeted NPs, PEG is located inside NP core and partly confined to the surface. The amount of PEG on the surface decreases for DBL<sub>L</sub> (despite their low size) and more in general upon addition of folate copolymer. Furthermore,  $[\Gamma]/[\Gamma^*]$  values well below the cut-off value of 1 indicate that PEG chains are in the mushroom-like conformation. These data demonstrate that, although NPs are prepared from PEGylated copolymers, the amount of PEG on the surface is below 7% in line with our previous results on triblock and star-shaped PEG-PCL copolymers (Ungaro et al., 2012). Similar degree of PEG coverage has been found preparing NPs by emulsion-solvent evaporation from mixtures of non-PEGylated and PEGylated copolymers (Xu et al., 2015).

The thickness of the external shell of NPs was evaluated by FALT, measuring the values of NPs  $\xi$  in NaCl solutions at different concentrations and fitting the data to a regression line ( $r > 0.980$ ) (Fig. 2A). The slope of these lines in absolute value represents FALT in nm. FALT is lower for NPs prepared from DBL<sub>S</sub> with short PEG ( $2.51 \pm 0.20$  nm) and higher for NPs prepared from DBL<sub>L</sub> with long PEG ( $3.84 \pm 0.15$  nm). In folate-decorated NPs, however, FALT increases for DBL<sub>S</sub>/DBL-Fol ( $2.72 \pm 0.11$  nm) and decreases for DBL<sub>L</sub>/DBL-Fol ( $3.58 \pm 0.29$  nm) suggesting a different arrangement of folate in the shell. Folate folding in PEG chains on the surface is likely occurring for DBL<sub>L</sub>/DBL-Fol, which could hide targeting ligand on the surface and prevent receptor recognition.

To gain insights into the environment experienced by folate moieties in the NPs, the emission behaviour of DBL<sub>S</sub>/DBL-Fol and DBL<sub>L</sub>/DBL-Fol was investigated by steady-state and time-resolved fluorescence spectroscopy. In fact, folate is a fluorescent molecule emitting in the visible range with an emission maximum at 450 nm. Fig. 2B shows the typical fluorescence emission of the folic acid, which is slightly more intense for DBL<sub>L</sub>/DBL-Fol. Inasmuch the two samples contain the same number of fluorogenic units, these slight but reproducible differences account for a larger fluorescence quantum yield for DBL<sub>L</sub>/DBL-Fol. In principle, this can be the result of i) self-quenching effects occurring in DBL<sub>S</sub>/DBL-Fol, ii) the different polarity experienced by the folate groups, or both. The dynamic behaviour of the fluorescence is in line with the former hypothesis. As shown in Table 3, the fluorescence decay was bi-exponential in both cases. However, we observed a more pronounced contribution of the longer component in the case of DBL<sub>L</sub>/DBL-Fol. These findings are in fairly good agreement with a picture involving the folate group of DBL<sub>S</sub>/DBL-Fol more exposed to water pool instead of being extended in the PEG shell.

### 3.3. Interaction of nanoparticles with HSA

Conformation of PEG on NPs surface can drive interactions with proteins. Here we focused on HSA, the most abundant protein in the blood pool. Interaction of NPs with HSA was clearly demonstrated by fluorescence spectroscopy. Fig. 3A shows the fluorescence spectra of HSA in the absence and in the presence of NPs upon excitation at 278 nm. This wavelength allows the selective excitation of HSA over folate. The black spectrum shows the typical dual band fluorescence spectrum of HSA, which reflects the contribution of the tyrosine ( $\lambda_{em}$  ca 310 nm) and tryptophan ( $\lambda_{em}$  ca 340 nm) fluorogenic centres. This strong emission is quenched by more than one order of magnitude upon addition of NPs. In contrast, the fluorescence of folate is basically

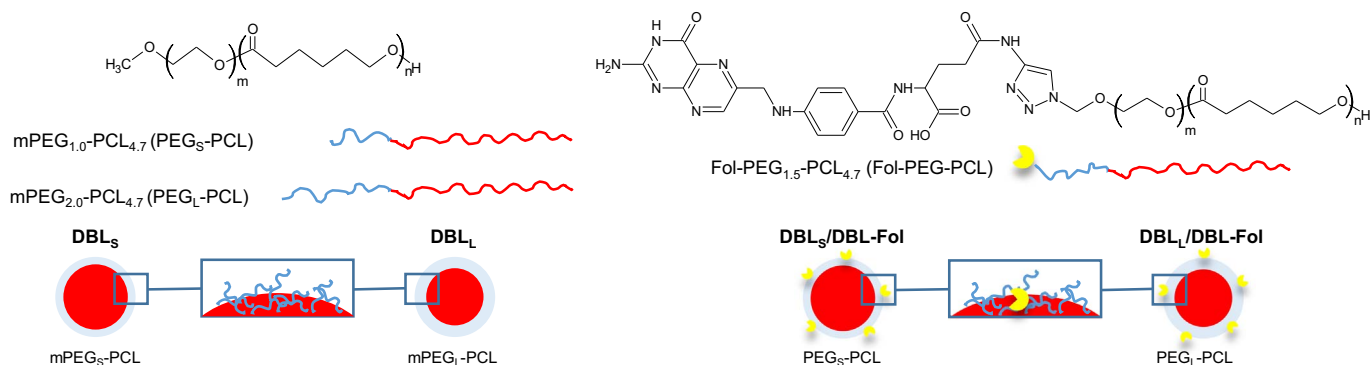


Fig. 1. Design of untargeted and targeted NPs prepared from PEG-PCL diblock copolymers with different PEG length.

Table 2

Properties of NPs prepared from short (DBL<sub>S</sub>) and long (DBL<sub>L</sub>) MPEG-PCL copolymers without and with Fol-PEG-PCL (DBL-Fol).

Formulation	D <sub>H</sub> <sup>a</sup> (nm)	PI	ξ (mV)	Surface PEG <sup>b</sup> (wt %)	[Γ] <sup>c</sup> (chains/100 nm <sup>2</sup> )	[Γ]/[Γ*] <sup>d</sup>
DBL <sub>S</sub>	78 ± 1	0.12	-13 ± 2	7.1	2.3	0.10
DBL <sub>S</sub> /DBL-Fol 20	82 ± 4	0.11	-18 ± 2	4.2	1.4	0.07
DBL <sub>L</sub>	34 ± 2	0.16	-15 ± 1	3.5	0.6	0.06
DBL <sub>L</sub> /DBL-Fol 20	59 ± 5	0.22	-17 ± 3	2.0	0.6	0.05

Values lower than 1 suggest a mushroom conformation. [Γ\*] represents the theoretical number of unconstrained PEG chains that would occupy the nanoparticle surface.

<sup>a</sup> The results are reported as mean of three separate measurements on three different batches ± SD.

<sup>b</sup> Surface PEG was measured by <sup>1</sup>H NMR integrals of PEG signals in copolymer solution and in NPs.

<sup>c</sup> [Γ] is the number of PEG chains per 100 nm<sup>2</sup> of nanoparticle surface area.

<sup>d</sup> The ratio [Γ]/[Γ\*] indicates packing extent of PEG on the surface.

unaffected in the presence of HSA (data not shown).

Since the emission of HSA fluorescent aminoacids well overlaps with the absorption spectrum of the folate, one could explain the quenching observed as a result of a photoinduced energy transfer via FRET mechanism. However, this is not the case since no emission of the folate was in fact observed concurrently to the quenching. Rather, the fluorescence behaviour might be simply due to static quenching effects arising by the massive aggregation of HSA on the NPs.

Formation of a HSA corona was evidenced also by evaluating size distribution curves of NPs at increasing HSA concentration (Fig. 3B). As compared to water, addition of HSA up to 5 μM does not change greatly the shape of the size curves, while at physiologically relevant HSA concentrations (500 μM) NPs mean size is increased for NPs of DBL<sub>L</sub> series and is unaltered for DBL<sub>S</sub>. The appearance of the peaks at 3 and 11 nm corresponding to free HSA monomers/tetramers/hexamers, indicate that in this adopted conditions, the surface of NPs is fully occupied by HSA. Remarkably, these results highlight that despite PEGylation, NPs developed here adsorb HSA forming a soft corona without inducing their aggregation.

### 3.4. Interaction of nanoparticles with human macrophages

To predict NPs *in vivo* capture by MPS once NPs are intravenously injected, we studied *in vitro* their uptake in human macrophages differentiated from monocytes and isolated from human buffy coats. Untargeted and folate-targeted NPs were not pre-incubated (time 0) or pre-incubated with human serum for 10 or 30 min at 37 °C before the addition and 3 h incubation with macrophages. A positive control of PCL NPs (non-PEGylated) was employed. Pre-incubation of NPs with

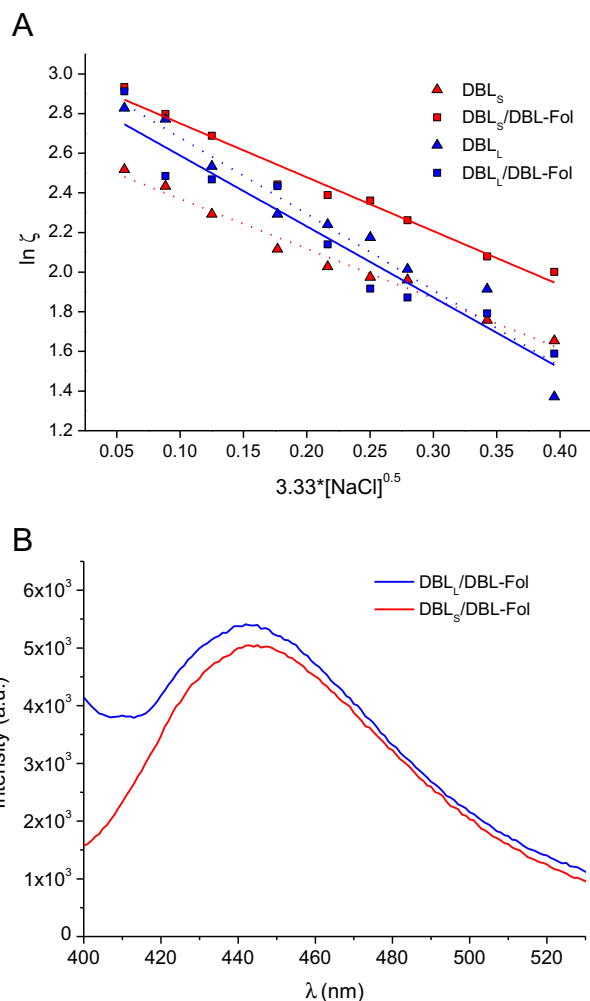
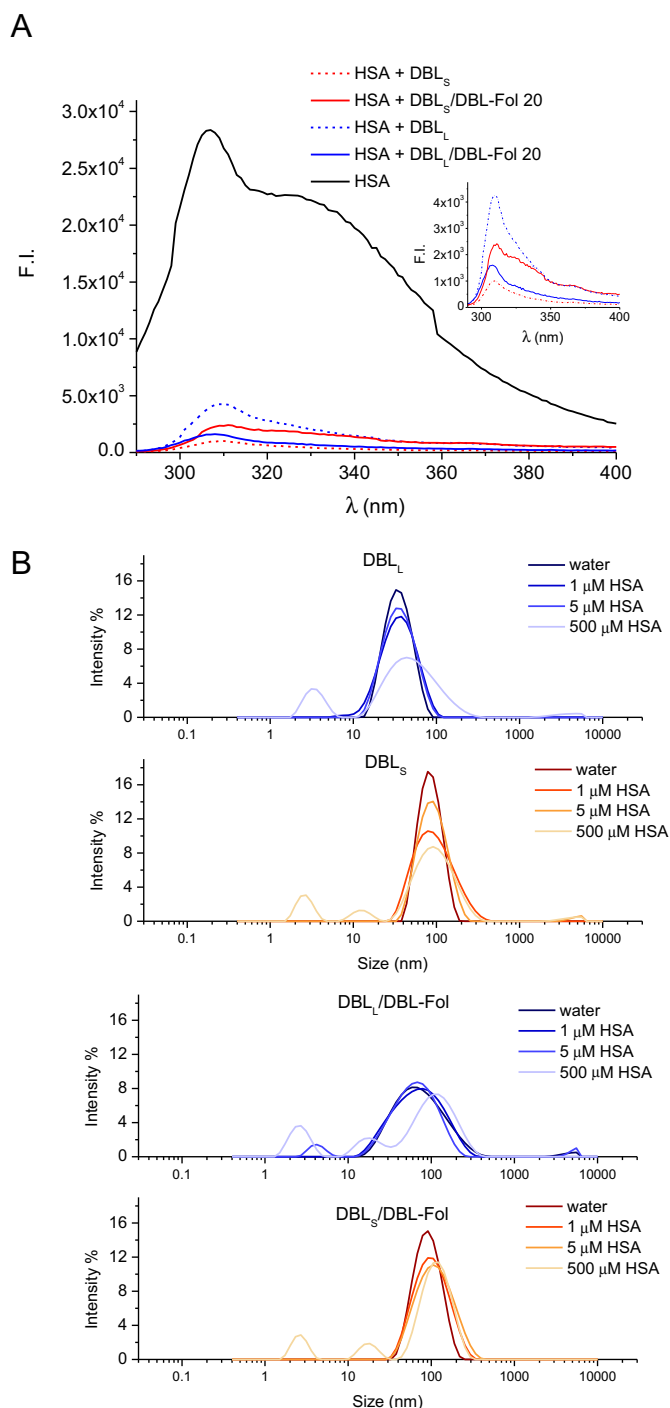


Fig. 2. Properties of the NPs shell. A) Thickness of the outer shell of non-targeted NPs (DBL<sub>S</sub> and DBL<sub>L</sub>) and targeted NPs (DBL<sub>S</sub>/DBL-Fol and DBL<sub>L</sub>/DBL-Fol). Shell thickness (in nm) can be derived from the absolute value of the slope in the regression lines. For clarity purpose, results of a single experiment are reported. B) Emission spectra of folate-decorated NPs (5 mg/mL) in water (λ<sub>exc</sub> = 370).

Table 3

Lifetimes (in ns) and amplitudes (Σα = 1) obtained by the biexponential fitting of the fluorescence decay for the different samples (λ<sub>exc</sub> = 370 nm λ<sub>em</sub> = 450 nm).

Sample	τ <sub>1</sub>	α <sub>1</sub>	τ <sub>2</sub>	α <sub>2</sub>
DBL <sub>S</sub> /DBL-Fol 20	0.50	0.30	7.71	0.70
DBL <sub>L</sub> /DBL-Fol 20	0.63	0.22	8.00	0.78



**Fig. 3.** Behaviour of NPs in the presence of HSA. A) Emission spectra of folate-decorated NPs (5 mg/mL) in the presence of HSA (3  $\mu$ M). A reference curve of a HSA solution (0.3  $\mu$ M) is reported for comparison. Excitation wavelength was 278 nm. B) Size distribution curves of NPs (0.05 mg/mL) in the presence of HSA (1–500  $\mu$ M).

human serum significantly increases their time-dependent uptake by macrophages for non-PEGylated NPs only (Fig. 4), while the uptake of all the PEGylated NPs is unaffected or shows the opposite trend. Confirming a general paradigm, non-PEGylated NPs demonstrate the highest capture level by macrophages. The uptake of untargeted NPs increases when shortening the PEG length from 2.0 kDa to 1.0 kDa. In any case, the presence of folate on the surface does not affect significantly NPs phagocytosis. These results are in line with the general observation that the presence of a PEG shell on NPs surface limits the adsorption of serum proteins largely preventing NPs capture by

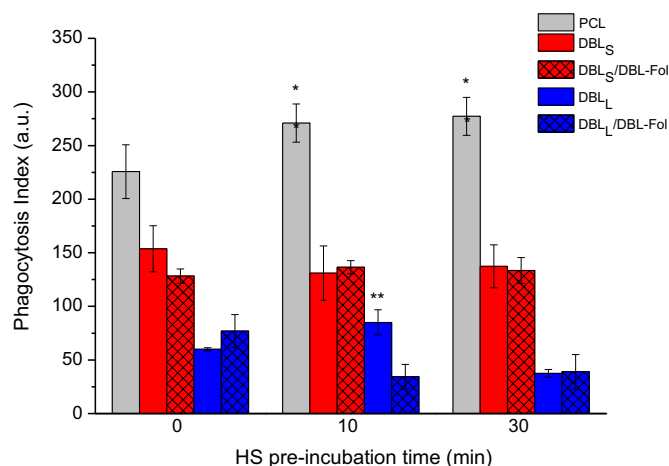


**Fig. 4.** NPs capture by macrophages. NPs were pre-incubated in human serum (HS) for 10 or 30 min before a 3 h incubation with macrophages at 37 °C. Phagocytosis Index represents the median total fluorescence intensity measured per macrophage by FACS. \* $p < 0.005$ , \*\* $p < 0.001$ , with respect to NPs not pre-incubated with human serum (Student's  $t$ -test).

phagocytes as macrophages (Walkey et al., 2012).

### 3.5. Cellular uptake of nanoparticles in KB cancer cells

To assess if the exposition of folate over the PEGylated surface increased the specific uptake of NPs in cells over-expressing FRs, we measured the uptake of targeted and non-targeted NPs in KB cells by flow cytometry. The uptake was measured in the absence and in the presence of 10% serum in the cell incubation medium to highlight the impact of NPs interaction with serum proteins. As reported in Fig. 5A, the uptake of DBL<sub>S</sub>/DBL-Fol occurs at least in part through FR-mediated endocytosis. In fact, pre-incubation of cells with 1 mM free Fol for 1 h to saturate FRs prior to NPs addition significantly decreases internalization. The extent of FR-mediated endocytosis of DBL<sub>S</sub>/DBL-Fol is higher without serum in the medium, probably due to partial 'masking effect' exerted by protein association to NPs shell (Conte et al., 2016). On the contrary, although PEGylation degree is low and PEG is in a mushroom conformation for both DBL<sub>S</sub>/DBL-Fol and DBL<sub>L</sub>/DBL-Fol, only DBL<sub>S</sub>/DBL-Fol allows the recognition of folate moieties by FR in the presence of serum. For DBL<sub>L</sub>/DBL-Fol, folate amount is lower than expected on the basis of fluorescence lifetimes, and is probably unable to extend over the NPs surface because of the presence of a serum proteins corona. Flow cytometry (Fig. 5A) and confocal microscopy analysis (Fig. 5B, C) confirm the capability of DBL<sub>S</sub>/DBL-Fol to be taken up by KB cells with some selectivity, especially in the absence of serum. Microscopy images highlight a cytoplasmic and more in particular a perinuclear localization of DBL<sub>S</sub>/DBL-Fol with a clear decrease of fluorescence signal in the case of cells pre-incubated with free folate.

On the contrary, in A549 cells negative for FR expression, flow cytometry experiments (Fig. S5) showed that the uptake of DBL<sub>S</sub> vs. DBL<sub>S</sub>/DBL-Fol was not significantly different ( $p > 0.05$ ,  $t$ -test) even in the absence of serum in the incubation medium. Accordingly, in spite of a slight decreased NP uptake observed in competition experiments with an excess of free folate, this decreased uptake was not statistically relevant comparing DBL<sub>S</sub> and DBL<sub>S</sub>/DBL-Fol ( $p > 0.05$ ,  $t$ -test).

To gain more insight into the mechanism of DBL<sub>S</sub>/DBL-Fol uptake in KB cells we used drugs widely employed as inhibitors of specific endocytic pathways as clathrin-mediated endocytosis (chlorpromazine hydrochloride, CHL), lipid-raft-dependent endocytosis (methyl- $\beta$ -cyclodextrin, Me $\beta$ CD) and caveolae-dependent endocytosis (Genistein, GEN and Filipin III, FIL). As reported in Fig. S6, Me $\beta$ CD significantly lowered NP uptake (~80%), indicating that also the majority of NPs which did not enter the cells via FRs (~30%) were taken up exploiting

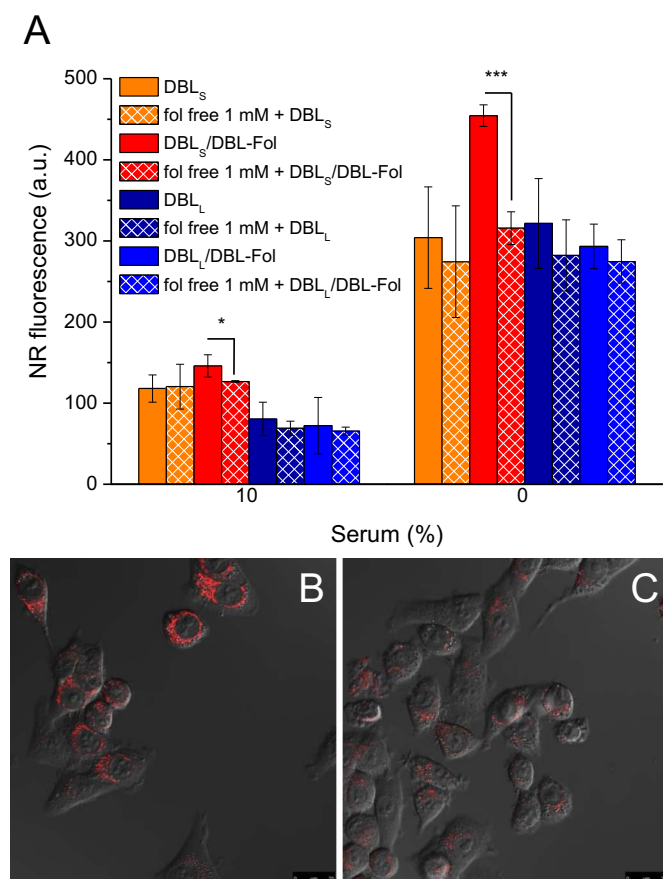


**Fig. 5.** Intracellular uptake of NPs in KB cells over-expressing FRs. Flow cytometry measurements of the uptake of 20  $\mu\text{g}/\text{mL}$  of Nile Red-loaded NPs (A). Cells were incubated with NPs for 1 h with or without 10% serum in the medium and in the absence or the presence of 1 mM free folate (competition experiment). Significant different for \* $p < 0.05$ , \*\*\* $p < 0.001$ , Student's *t*-test. Confocal images of cells incubated with DBL<sub>S</sub>/DBL-Fol in the absence (B) or in the presence (C) of 1 mM free folate. (For interpretation of the references to color in this figure legend, the reader is referred to the web version of this article.)

lipid raft-dependent endocytosis. On the other hand, neither chlorpromazine nor Genistein nor Filipin were able to inhibit DBL<sub>S</sub>/DBL-Fol NP uptake, indicating that clathrin-mediated and caveolae-dependent endocytosis were not involved in the cell internalization process.

### 3.6. Modulating degree of valency in folate-decorated nanoparticles based on mPEG<sub>5</sub>-PCL

As a final experiment, we prepared DBL<sub>S</sub>/DBL-Fol at different folate copolymer percentage (0–50% by wt of total copolymer) to understand if the amount of folate copolymer affected uptake in KB cells. Size distribution curves indicate that all the formulations are monodispersed (Fig. 6A) with a size below 100 nm up to 30% of folate copolymer. A trend towards an increase of mean size and PI is observed for NPs at 50% Fol-PEG-PCL. All the NPs show a negative surface ( $\xi$  potential from  $-13$  to  $-18$  mV) as generally found for PEGylated NPs. As it can be seen in Fig. 6B, emission intensity of NPs is increased when increasing folate content whereas NPs of PEG<sub>5</sub>-PCL (without folic acid) do not exhibit any fluorescence signal. Furthermore, increase of Fol-PEG-PCL to 50% does not increase significantly NPs fluorescence, confirming that a fluorescence quenching is observed when the surface is more populated by folate moieties. Uptake studies in KB cells incubated with DBL<sub>S</sub>/DBL-Fol containing 10%, 20% or 30% DBL-Fol polymers (Fig. 6C) demonstrated that, even in the presence of serum all the folate targeted formulations are taken up by cells via FR $\alpha$ -mediated endocytosis.

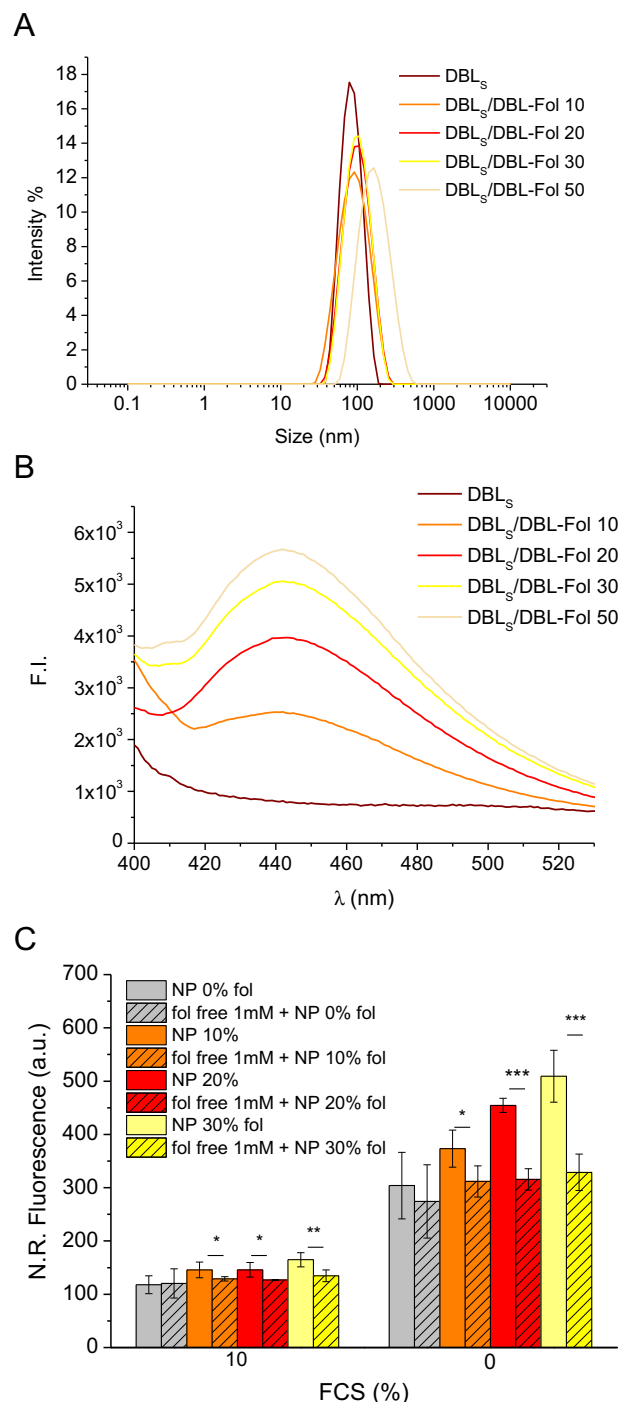


**Fig. 6.** Properties of DBL<sub>S</sub>/DBL-Fol NPs with different percentages of Fol-PEG-PCL. A) Size distribution curves. B) Emission spectra at  $\lambda_{\text{exc}} = 278$  nm (NPs concentration was 5 mg/mL). C) Uptake of NR-loaded NPs (20  $\mu\text{g}/\text{mL}$ ) in KB cells after 1 h incubation in the presence and absence of FCS.

Nevertheless, the extent of NPs accumulation through FR $\alpha$ -mediated endocytosis was comparable for all the formulations suggesting that an increase of folate amount in the NPs does not improve the extent of NPs intracellular accumulation.

## 4. Conclusions

Our study highlights that the too simplistic view of PEGylated NPs, both untargeted and targeted, is out to be close to the actual situation and needs to be elucidated if one wishes to correlate appropriately NPs

properties to biological behaviour. We demonstrate that NPs prepared from diblock PEG-PCL copolymers by the widely employed solvent displacement method show a degree of PEGylation much lower than expected which depends on the length of PEG block. PEG acquires a mushroom conformation on NPs surface and its length affects the thickness of the hydrophilic shell as well as folate amount and exposition. HSA interacts with all NPs forming a protein corona which is not detrimental for stability. While all NPs show limited uptake in human macrophages, only the presence of short PEG (1.0 kDa) in the copolymer ensures that folate-bearing NPs are accumulated in KB cancer cells via FR $\alpha$ -mediated endocytosis.

This study offers a proof on how complimentary and simple techniques such as light scattering, fluorescence and NMR, can be employed to finely characterize the shell of targeted NPs with a PEGylated surface in the attempt to drive downstream effect such as NPs internalization in sub-set cell populations.

## Acknowledgments

This work was supported by Italian Association for Cancer Research (IG2014 #15764). The authors thank Mrs. D. Melck (NMR Service of Institute of Biomolecular Chemistry, CNR, Pozzuoli, Italy) for technical assistance. The authors are indebted to Prof. M. Trifuoggi (ACE Laboratory, University of Naples Federico II, Italy) for MP-AES analysis.

## Appendix A. Supplementary data

Supplementary data to this article can be found online at <https://doi.org/10.1016/j.ejps.2017.09.048>.

## References

- Auguste, D.T., Armes, S.P., Brzezinska, K.R., Deming, T.J., Kohn, J., Prud'homme, R.K., 2006. pH triggered release of protective poly(ethylene glycol)-b-polycation copolymers from liposomes. *Biomaterials* 27, 2599–2608.
- Bertrand, N., Leroux, J.C., 2012. The journey of a drug-carrier in the body: an anatomophysiological perspective. *J. Control. Release* 161, 152–163.
- Cammass, S., Nagasaki, Y., Kataoka, K., 1995. Heterobifunctional poly(ethylene oxide): synthesis of alpha-methoxy-omega-amino and alpha-hydroxy-omega-amino PEOs with the same molecular weights. *Bioconjug. Chem.* 6, 226–230.
- Cao, B., Zheng, Y., Xi, T., Zhang, C., Song, W., Burugapalli, K., Yang, H., Ma, Y., 2012. Concentration-dependent cytotoxicity of copper ions on mouse fibroblasts in vitro: effects of copper ion release from TCu380A vs TCu220C intra-uterine devices. *Biomed. Microdevices* 14, 709–720.
- Chen, C., Ke, J., Zhou, X.E., Yi, W., Brunzelle, J.S., Li, J., Yong, E.-L., Xu, H.E., Melcher, K., 2013. Structural basis for molecular recognition of folic acid by folate receptors. *Nature* 500, 486–489.
- Cheung, A., Bax, H.J., Josephs, D.H., Iliev, K.M., Pellizzari, G., Opzoomer, J., Bloomfield, J., Fittall, M., Grigoriadis, A., Figini, M., Canevari, S., Spicer, J.F., Tutt, A.N., Karagiannis, S.N., 2016. Targeting folate receptor alpha for cancer treatment. *Oncotarget*.
- Conte, C., Fotticchia, I., Tirino, P., Moret, F., Pagano, B., Gref, R., Ungaro, F., Reddi, E., Giancola, C., Quaglia, F., 2016. Cyclodextrin-assisted assembly of PEGylated polyester nanoparticles decorated with folate. *Colloids Surf. B: Biointerfaces* 141, 148–157.
- El-Gogary, R.I., Rubio, N., Wang, J.T.-W., Al-Jamal, W.T., Bourgonon, M., Kafa, H., Naeem, M., Klippstein, R., Abbate, V., Leroux, F., Bals, S., Van Tendeloo, G., Kamel, A.O., Awad, G.A.S., Mortada, N.D., Al-Jamal, K.T., 2014. Polyethylene glycol conjugated polymeric nanocapsules for targeted delivery of quercetin to folate-expressing cancer cells in vitro and in vivo. *ACS Nano* 8, 1384–1401.
- Endres, T.K., Beck-Broichsitter, M., Samsonova, O., Renette, T., Kissel, T.H., 2011. Self-assembled biodegradable amphiphilic PEG-PCL-IPEI triblock copolymers at the borderline between micelles and nanoparticles designed for drug and gene delivery. *Biomaterials* 32, 7721–7731.
- Gao, H., Yang, Z., Zhang, S., Pang, Z., Jiang, X., 2014. Internalization and subcellular fate of aptamer and peptide dual-functionalized nanoparticles. *J. Drug Target.* 22, 450–459.
- Grossen, P., Witzigmann, D., Sieber, S., Huwyler, J., 2017. PEG-PCL-based nanomedicines: a biodegradable drug delivery system and its application. *J. Control. Release* 260, 46–60.
- Hiki, S., Kataoka, K., 2007. A facile synthesis of azido-terminated heterobifunctional poly(ethylene glycol)s for “Click” conjugation. *Bioconjug. Chem.* 18, 2191–2196.
- Himo, F., Lovell, T., Hilgraf, R., Rostovtsev, V.V., Noodleman, L., Sharpless, K.B., Fokin, V.V., 2005. Copper(I)-catalyzed synthesis of azoles. DFT study predicts unprecedented reactivity and intermediates. *J. Am. Chem. Soc.* 127, 210–216.
- Ishii, T., Yamada, M., Hirase, T., Nagasaki, Y., 2005. New synthesis of heterobifunctional poly(ethylene glycol) possessing a pyridyl disulfide at one end and a carboxylic acid at the other end. *Polym. J.* 37, 221–228.
- Li, Z., Chau, Y., 2010. Synthesis of heterobifunctional poly(ethylene glycol)s by an acetal protection method. *Polym. Chem.* 1, 1599–1601.
- Li, Z., Tan, B.H., 2014. Towards the development of polycaprolactone based amphiphilic block copolymers: molecular design, self-assembly and biomedical applications. *Mater. Sci. Eng. C* 45, 620–634.
- Liu, L., Zheng, M., Renette, T., Kissel, T., 2012. Modular synthesis of folate conjugated ternary copolymers: polyethylenimine-graft-polycaprolactone-block-poly(ethylene glycol)-folate for targeted gene delivery. *Bioconjug. Chem.* 23, 1211–1220.
- Mahou, R., Wandrey, C., 2012. Versatile route to synthesize heterobifunctional poly(ethylene glycol) of variable functionality for subsequent pegylation. *Polymer* 4, 561.
- Nahrwold, M., Weiß, C., Bogner, T., Mertink, F., Conradi, J., Sammet, B., Palmisano, R., Royo Gracia, S., Preuß, T., Sewald, N., 2013. Conjugates of modified cryptophycins and RGD-peptides enter target cells by endocytosis. *J. Med. Chem.* 56, 1853–1864.
- Owens 3rd, D.E., Peppas, N.A., 2006. Opsonization, biodistribution, and pharmacokinetics of polymeric nanoparticles. *Int. J. Pharm.* 307, 93–102.
- Quaglia, F., Ostacolo, L., De Rosa, G., La Rotonda, M.I., Ammendola, M., Nese, G., Maglio, G., Palumbo, R., Vauthier, C., 2006. Nanoscopic core-shell drug carriers made of amphiphilic triblock and star-diblock copolymers. *Int. J. Pharm.* 324, 56–66.
- Rabanel, J.M., Hildgen, P., Banquy, X., 2014. Assessment of PEG on polymeric particles surface, a key step in drug carrier translation. *J. Control. Release* 185, 71–87.
- Raynaud, J., Absalon, C., Gnanou, Y., Taton, D., 2009. N-Heterocyclic carbene-induced zwitterionic ring-opening polymerization of ethylene oxide and direct synthesis of  $\alpha,\omega$ -difunctionalized poly(ethylene oxide)s and poly(ethylene oxide)-b-poly( $\epsilon$ -caprolactone) block copolymers. *J. Am. Chem. Soc.* 131, 3201–3209.
- Szekely, G., Schaepertoes, M., Gaffney, P.R.J., Livingston, A.G., 2014. Iterative synthesis of monodisperse PEG homostars and linear heterobifunctional PEG. *Polym. Chem.* 5, 694–697.
- Thompson, M.S., Vadala, T.P., Vadala, M.L., Lin, Y., Riffle, J.S., 2008. Synthesis and applications of heterobifunctional poly(ethylene oxide) oligomers. *Polymer* 49, 345–373.
- Tirino, P., Conte, C., Ordegno, M., Palumbo, R., Ungaro, F., Quaglia, F., Maglio, G., 2014. Y- and H-shaped amphiphilic PEG-PCL block copolymers synthesized combining ring-opening polymerization and click chemistry: characterization and self-assembly behavior. *Macromol. Chem. Phys.* 215, 1218–1229.
- Trindade, A.F., Frade, R.F.M., Macoas, E.M.S., Graca, C., Rodrigues, C.A.B., Martinho, J.M.G., Afonso, C.A.M., 2014. “Click and go”: simple and fast folic acid conjugation. *Org. Biomol. Chem.* 12, 3181–3190.
- Ungaro, F., Conte, C., Ostacolo, L., Maglio, G., Barbieri, A., Arra, C., Misso, G., Abbruzzese, A., Caraglia, M., Quaglia, F., 2012. Core-shell biodegradable nanoassemblies for the passive targeting of docetaxel: features, antiproliferative activity and in vivo toxicity. *Nanomedicine* 8, 637–646.
- Viola-Villegas, N., Rabideau, A.E., Cesnavicius, J., Zubieta, J., Doyle, R.P., 2008. Targeting the folate receptor (FR): imaging and cytotoxicity of Rel conjugates in FR-overexpressing cancer cells. *ChemMedChem* 3, 1387–1394.
- Walkey, C.D., Olsen, J.B., Guo, H., Emili, A., Chan, W.C., 2012. Nanoparticle size and surface chemistry determine serum protein adsorption and macrophage uptake. *J. Am. Chem. Soc.* 134, 2139–2147.
- Xu, Q., Ensign, L.M., Boylan, N.J., Schon, A., Gong, X., Yang, J.C., Lamb, N.W., Cai, S., Yu, T., Freire, E., Hanes, J., 2015. Impact of surface polyethylene glycol (PEG) density on biodegradable nanoparticle transport in mucus ex vivo and distribution in vivo. *ACS Nano* 9, 9217–9227.